# Co-opting Mobile Device Cellular RF Front Ends for HCI Sensing

Daehwa Kim
School of Computer Science
Carnegie Mellon University
Pittsburgh, Pennsylvania, USA
daehwak@cs.cmu.edu

Chris Harrison
School of Computer Science
Carnegie Mellon University
Pittsburgh, Pennsylvania, USA
chris.harrison@cs.cmu.edu

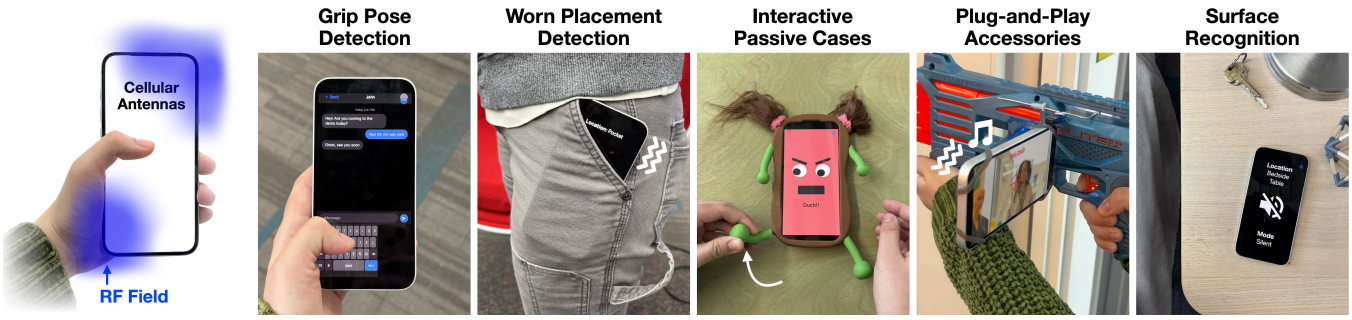



**Figure 1: We show that smartphone cellular RF front ends can serve as versatile sensors, enabling a wide range of applications such as grip pose sensing, worn placement detection, passive-yet-interactive cases, plug-and-play accessory experiences, and surface recognition. Although these capabilities have previously been explored in the HCI literature, often using specialized hardware, we demonstrate that they can be realized using capabilities already present in ubiquitous smartphones.**

## Abstract

Modern smartphones contain sophisticated cellular modems that can tune their antennas. We show how this latent internal capability, intended to minimize power consumption while maximizing antenna performance, can be co-opted as a sensing capability in already ubiquitous mobile devices. For example, we can sense electromagnetic loading from a user's hand, surrounding objects, and nearby materials, enabling diverse applications such as detecting grip pose, worn device placement, and passive interactive widgets. As a proof of concept, we selected five example use cases from the HCI literature, created with different and specialized sensors, and re-implemented them with a commercial off-the-shelf smartphone. We use these to evaluate sensing performance, comparing to prior work, and the results underscore the promise and generalizability of smartphone RF hardware as a future sensing modality.

## Keywords

Mobile, Smartphone, Smartwatch, Cellular, Modem, RF, RFFE, Radio Frequency, Sensing, Around Device Interaction.

**ACM Reference Format:**
Daehwa Kim and Chris Harrison. 2026. Co-opting Mobile Device Cellular RF Front Ends for HCI Sensing. In *The 39th Annual ACM Symposium on User Interface Software and Technology (UIST '26), November 02–05, 2026, Detroit, MI, USA.* ACM, New York, NY, USA, 14 pages. https://doi.org/10.1145/3830398.3830594

This work is licensed under a Creative Commons Attribution-NonCommercial-NoDerivatives 4.0 International License.
*UIST '26, Detroit, MI, USA*
© 2026 Copyright held by the owner/author(s).
ACM ISBN 979-8-4007-2856-3/26/11
https://doi.org/10.1145/3830398.3830594

## 1 Introduction

Modern mobile devices, most notably smartphones (but also some smartwatches, tablets, and laptops), contain sophisticated radio frequency front-ends (RFFE) for cellular communication. These enable reliable and power-efficient wireless connectivity, automatically compensating for factors such as environmental loading, user interaction, and device orientation. Unlike early mobile radios that relied on static antenna-matching architectures, contemporary modems continuously monitor transmitted and reflected RF power and actively reconfigure antenna behavior using integrated impedance and aperture tuners [43–45, 53].

This dynamic tuning capability implicitly enables sensing of antenna behavior, including changes induced by proximate external electromagnetic loading. By operating across multiple cellular frequency bands, the modem can further probe antenna response as a function of frequency. Conceptually, this process mirrors the operation of a vector network analyzer (VNA), which characterizes RF components by sweeping frequencies and measuring reflected and transmitted signals, particularly antenna reflection (i.e., S11). While smartphone RFFE subsystems are designed for communication rather than precision RF instrumentation, their ability to programmatically observe frequency-dependent antenna performance provides a VNA-like sensing capability *already embedded* within commodity consumer devices.

Simultaneously, prior research in Human-Computer Interaction (HCI) has demonstrated that RF measurements obtained from VNAs can serve as a powerful sensing modality [2, 20–22, 55, 57, 60]. These works established that antenna impedance measurements are sensitive to human hand pose [20, 22, 57, 59], face pose [21], environmental interaction and nearby widgets [2, 55, 60]. However, these approaches have relied on specialized laboratory instrumentation and custom RF hardware, limiting their scalability and deployment.

In this paper, we present the first demonstration that RF sensing for HCI applications can be realized using the existing RFFE hardware already embedded in mobile devices. Unlocking RF sensing on widely deployed consumer devices significantly expands the accessibility and scalability of RF-driven HCI interaction techniques. This insight not only offers a pathway for prior VNA-based interaction paradigms to move beyond laboratory prototypes, but also introduces new opportunities for continuous, real-world, and context-aware sensing scenarios that leverage the pervasive presence of mobile devices. By reframing communication subsystems as sensing infrastructure, our work demonstrates how latent RF reconfigurability in commodity hardware can serve as a new avenue for ubiquitous interactive sensing.

To demonstrate the feasibility and generality of our idea, we re-implement five use cases previously motivated and demonstrated in the HCI literature, using an off-the-shelf smartphone. We then use these functional implementations to evaluate sensing performance, which we can directly compare with prior work implementing similar functionality. Our experiments show that commonplace mobile hardware can achieve sensing accuracy comparable to prior work, while operating from a standard device rather than hardware tailored to individual use cases.

## 2 Related Work & Background

We now review four diverse areas of related work. First, we provide some background on radio frequency front-ends and the components they incorporate to monitor and tune their antennas. Next we briefly review other HCI papers that share the long-standing mantra of re-purposing hardware intended for one use to enable unanticipated new uses. We then briefly cover the conceptually related HCI subfield of Around-Device Interaction. Finally, we conclude with a discussion of prior work most technically related to our own: other HCI works employing EM and RF sensing.

### 2.1 Radio Frequency Front Ends

Modern smartphones incorporate highly sophisticated radio frequency front-end (RFFE) subsystems that enable efficient operation across dozens of cellular, WiFi, Bluetooth, and GNSS frequency bands. The RFFE sits between the baseband transceiver and the antenna system and is responsible for conditioning signals for transmission and reception. Core components of the RFFE typically include power amplifiers (PAs), low-noise amplifiers (LNAs), filters, duplexers, switches, tunable matching networks, and antenna selection or diversity elements. A representative example block diagram is offered in Figure 2. Together, these components optimize signal integrity, spectral compliance, and power efficiency while compensating for dynamic environmental factors such as user grip, device orientation, and nearby materials. These capabilities are publicly described by wireless modem manufacturers, including Qualcomm [44, 45], Qorvo [43], and Skyworks [53].

Unlike earlier fixed matching architectures, contemporary RFFE designs rely heavily on adaptive tuning networks. Smartphone antennas operate in extremely constrained physical volumes and must maintain acceptable impedance matching across wide frequency ranges. Because the electromagnetic environment surrounding a handset changes continuously during use, modern devices dynamically reconfigure their antenna matching and routing paths. These reconfigurations occur at runtime under control of the baseband modem and RFFE controller, allowing the device to maintain high radiated efficiency and regulatory compliance.

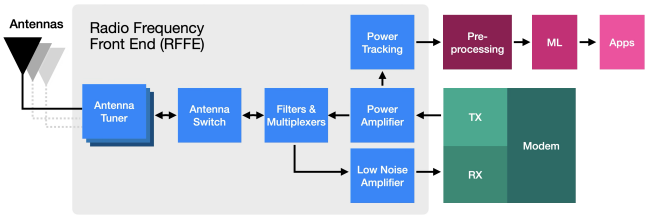



**Figure 2: Block diagram showing the major components of a typical cellular modem (adapted from [46]). Our software interfaces with the power tracking features of the RFFE, passing data to machine learning to power interactive features.**

Recent advances in RFFE silicon have introduced highly integrated tunable elements that provide fine-grained control over antenna behavior. Commercial components such as impedance tuners, aperture tuners, and antenna diversity switches provide programmable control over antenna matching and radiation characteristics. For instance, impedance tuners, such as Qualcomm's QAT3550 [52], incorporate digitally controlled reactive elements that dynamically adjust antenna matching networks. These devices typically employ switched capacitor banks or variable reactance structures that allow the system to optimize antenna impedance under varying loading conditions. By modifying the matching network, the tuner can maximize power transfer between the RF chain and the antenna while minimizing reflection losses. Aperture tuners (e.g., QAT3514 [52]) modify the effective electrical length or radiating characteristics of antenna structures. Rather than adjusting impedance directly, aperture tuning alters the antenna's resonant properties, effectively shifting operational frequency bands or improving radiation efficiency across multi-band operation. This form of tuning is particularly valuable in compact smartphone form factors where a single antenna must support multiple frequency allocations. Antenna switches, such as the QAT3522 [52], provide dynamic routing between multiple antenna elements. These switches allow the modem to select among spatially distributed antennas or antenna types to improve link robustness and mitigate detuning effects caused by user interaction or environmental obstruction.

RFFEs rely on internal RF power measurements to decide when and how to retune. During transmission, directional couplers or related detector circuits sample the forward power delivered by the power amplifier and, in some architectures, the power reflected back from the antenna due to impedance mismatch. These measurements provide a direct indication of how efficiently RF energy is being transferred into the antenna under current loading conditions. The modem and RFFE controller use this feedback in a closed loop to select updated tuner states, antenna paths, or matching-network configurations that reduce reflection and improve radiated performance. Separately, envelope-tracking circuitry dynamically adjusts the power amplifier supply voltage to follow the instantaneous transmit envelope, improving transmitter efficiency while the tuning loop optimizes the antenna interface. Together, these




**Figure 3: For each antenna, we measure performance at 3 frequencies across 5 different LTE and 5G cellular bands (B1, B3, B7, B30, N25), spanning from 1.7 to 2.6 GHz.**

feedback and control mechanisms allow modern smartphones to adapt transmission behavior in real time as user interaction and the surrounding environment detune the antenna system.

RFFE components are typically programmable through control interfaces exposed within the modem and RFFE controller stack. Access to these controls is usually restricted to device manufacturers and platform integrators via proprietary firmware interfaces and vendor-specific application programming interfaces (APIs). Smartphone reference platforms, like Qualcomm's popular Snapdragon series, also provide access to these subsystems. To complete this investigation, we developed a software application that interfaces with the cellular modem's power monitoring subsystem.

## 2.2 Repurposing Hardware for Sensing

A longstanding theme in HCI and at ACM UIST is the repurposing of commodity hardware for sensing, where existing components in commercial off-the-shelf (COTS) devices are used to infer user actions, body states, or environmental context in ways never intended by the original hardware design. A key appeal of this approach is that it often requires only software-level reinterpretation of existing signals, avoiding the need for custom instrumentation. Prior work has demonstrated this across many sensing modalities and use cases: device speakers and microphones have been repurposed for interaction sensing [11, 38, 54], ECG sensors for communication with accessories [58], PPG sensors for augmenting touch input of non-touchscreens [72], device vibration motors and IMUs have enabled grip-sensing [9], IMUs have also been used to detect tool use [30] and vibration-based communication [69], magnetometers have supported around-device input [14, 40], capacitive touchscreens have been repurposed for authentication [10, 16] and multi-device interaction [67], and WiFi radios have been used for human and physiological sensing [1, 42]. Our work follows this tradition by repurposing cellular antenna impedance tuning, a mechanism originally designed for improving communication, as a modality for near-device interaction.

## 2.3 Around-Device Interaction

Around-device interaction (ADI) has been widely explored as a way to extend interaction beyond the limited input space available on mobile and wearable devices. Prior work extends this via sensing hand grip/gesture [5, 9, 31, 74, 77, 78, 81], adding additional widgets (e.g., button, slider, toy arm, pen) [18, 19, 28, 56, 75], or augmenting applications considering worn/off-body locations [9, 13, 62, 73]. These uses have been achieved via a broad range of sensing modalities, including proximity-based sensing [3, 27, 29], magnetic tracking [14, 18, 19, 75], camera-based approaches [5, 74, 77], and both active and passive acoustic sensing [12, 28, 38, 49, 56, 68]. Our work builds on this line of research with a new means of sensing.

## 2.4 EM & RF Sensing in HCI

Electromagnetic (EM) and radio frequency (RF) sensing are closely related to our approach and have been explored in HCI as alternatives to conventional touch- and vision-based sensing. These techniques enable the sensing of interaction while mitigating occlusion, fitting within compact form factors, and enabling novel forms of input. Prior work has investigated capacitive sensing through both direct touch [80, 81] and near-field sensing [15, 31] to augment mobile device touch input. Because EM signals are also highly sensitive to the human body, researchers have further explored both on-body and through-body sensing for interaction, tracking, and user identification [25, 26, 48, 79, 82, 83]. Researchers have also explored radar-based sensing for interaction, including material classification, worn-location detection for context sensing, and gesture recognition [36, 61, 73].

More closely related to our work, several systems have used resonance and impedance properties themselves as an interaction primitive. Early work explored resonant tuning and swept-frequency techniques to sense touch and object interaction through changes in electrical resonance [39, 41, 48, 55]. Closest to our approach, a growing body of work has used antenna or RF-channel measurements, including S-parameters, as a sensing signal for interaction and body-pose recognition [2, 20–22, 33, 57, 59, 60, 70]. These systems show that RF impedance and transmission characteristics can encode rich information about touch, pose, and body proximity.

To the best of our knowledge, our work is the first to demonstrate interactive RF sensing using cellular RF front ends that are already built into commercial smartphones. Rather than relying on custom or dedicated RF hardware, we repurpose the phone's existing antenna-tuning mechanism, originally designed to support wireless communication, as a sensing modality. Further, we show that this approach can enable a range of applications previously explored with specialized hardware.

# 3 Implementation

Our implementation relies on latent smartphone hardware capabilities, accessed by our software, which provides a VNA-like sensor stream. This is then interpreted by machine learning models to power interactive end-user functionality. We describe five example use cases in Section 4. In this section, we now describe the major components of our system.

## 3.1 RFFE as a Low-Fidelity VNA for Sensing

As already discussed, the programmability of modern RFFEs enables direct interrogation of antenna performance using hardware already embedded within smartphones. By orchestrating sweeps across multiple frequencies (e.g., LTE bands), the RFFE can effectively be used to probe antenna reflection characteristics across

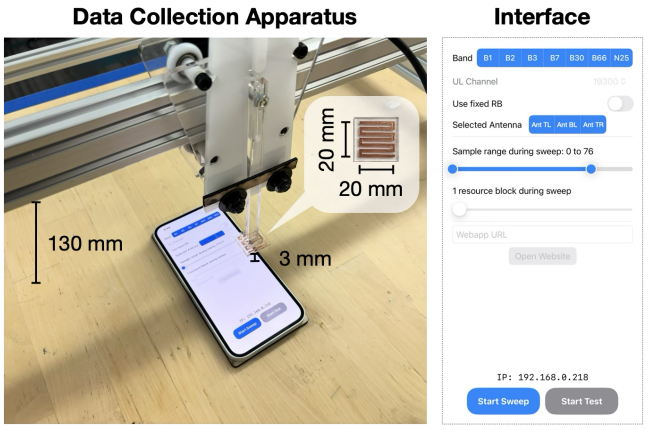



**Figure 4: Left: CNC apparatus for probing the smartphone's RF field. We use a wide-band monopole antenna, measuring 20 × 20 mm, which was incrementally translated 3 mm above the phone screen, across a 140 × 215 mm area. Cellular antenna performance was measured at each position, producing a spatial visualization of antenna performance (Figure 5). Right: Screenshot of our RFFE control interface.**

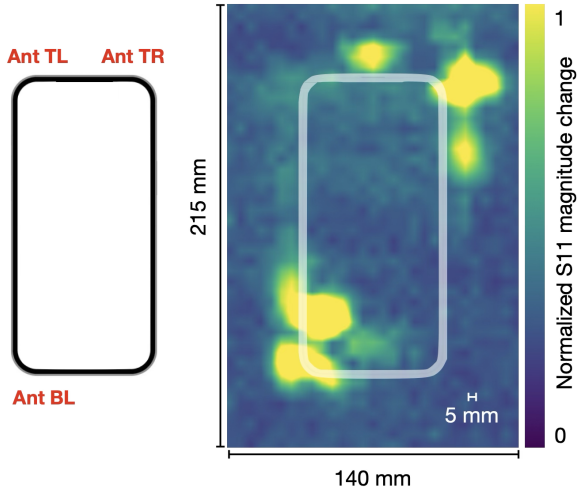



**Figure 5: Heatmap of S11 change in response to a proximate antenna (see setup in Figure 4). It is apparent that the sensing range is limited to the immediate volume around the device, ideal for applications such as grip pose and surface recognition. Longer-range use cases appear infeasible at present.**

portions of the RF spectrum. This process is conceptually analogous to traditional vector network analyzers (VNAs), which measure scattering parameters by injecting known RF signals and measuring reflected and transmitted responses across a range of frequencies. While smartphone RFFE systems cannot directly measure full complex scattering matrices with laboratory-grade precision, they can approximate frequency-dependent antenna response using internal diagnostic measurements.

## 3.2 Cellular Band Selection

The smartphone we use can communicate on many LTE [64] and 5G [63] uplink bands. Bands can overlap substantially (e.g., B3 and N25), and thus provide redundant information. We selected five useful, non-overlapping bands to sense (B1, B3, B7, B30, and N25), which include frequency ranges that cover 1.7 to 2.6 GHz, depicted in Figure 3. Our RFFE allows us to probe these bands on any of the phone's antennas (by commanding the antenna switch), although each of the antennas is optimized for different sets of bands.

The RFFE allows us to capture hundreds of measurements within a single band, evenly spaced. While such fine spectral resolution is useful in cellular systems, where devices may operate on many narrow channels within a band, it is less critical for our uses as electromagnetic loading from, e.g., a user's hand is comparatively broadband. Thus, for each of the five LTE/5G bands we use, we measure antenna matching behavior (S11) at three frequencies: the band's start and end frequencies, as well as the band's center frequency. This means for each antenna we sample 5 bands × 3 frequencies = 15 complex values (magnitude and phase) from 1710 to 2560 MHz. Note these are not evenly distributed, as illustrated in Figure 3.

We note that some smartphones, especially global variants, have support for dozens of bands that could allow for more regular and wider sampling of frequencies. For example, the global variant of the Galaxy S25 Ultra (model SM-S938B) has support for 20 LTE bands and 17 5G NR bands [8]. Also, it is entirely possible that the RFFE hardware can measure intermediate (i.e., non-band) frequencies, but this is not exposed to developers.

## 3.3 Antenna Selection

It is not uncommon for modern flagship devices to contain three or more antennas for cellular communication, with several other antennas supporting Bluetooth, WiFi, GPS, and other standards [4, 7, 17]. In some cases, different antennas operate across the same bands, but with different polarizations, and other times, different antennas are utilized for different cellular bands. Antenna redundancy is helpful to mitigate interference from specific user grips and maximize performance across device orientations.

From public FCC filings, we can see, for example, even budget-friendly phone models such as the Samsung Galaxy M35 5G [47] and TCL 10 5G [65] contain three cellular antennas, arrayed around the frame of the phone. The phone we use also has three antennas located in the corners (top-left, TL; bottom-left, BL; top-right, TR), as illustrated in Figure 5. These antennas support sensing across all five cellular bands we selected in the previous subsection.

## 3.4 RFFE Sensing

We created a basic application (Figure 4, right) to interface with the phone's RFFE and stream live measurements over a socket to a laptop, where we could conveniently visualize and record data. Importantly, this means we could operate the phone in an untethered fashion, avoiding confounds introduced by grounding.

For a single antenna, we capture 15 measurements (5 bands × 3 frequencies). We repeat this process for two more antennas. Note that each S11 measurement contains two values: magnitude and phase. In total, a complete new frame of 90 values takes ~2.5 sec to capture. However, we update our data every time a band is

read (three measurements) and we run our machine learning (discussed in the next section) at this interval. We note that triggering measurements sequentially through our current implementation is sub-optimal; a more integrated implementation could achieve higher frame rates. Nonetheless, we believe our present implementation is sufficient to validate the idea; better APIs would increase frame rate, but not necessarily accuracy.

## 3.5 Machine Learning & Featurization

The final step of our pipeline, before passing events to end-user applications, is the interpretation of our signals by a machine learning model. We employ three feature encoding strategies as input to our machine learning models. First, we use the complex reflection coefficient ($S11$) directly to capture geometric properties (e.g., hand shape), resulting in 2 feature channels (1 real and 1 imaginary component of $S11$). Second, we convert $S11$ into impedance representation ($50\frac{1+S11}{1-S11}$) to measure the tissue's physical energy absorption and proximity capacitance, and our model takes the two coefficients of this complex number as additional features. Lastly, we represent $S11$ in polar form using magnitude ($20\log_{10}|S11|$) and phase ($\frac{image(S11)}{real(S11)}$) to incorporate the resonance detuning and signal delay caused by the dielectric presence. As the phase is circular, we further encode it using sine and cosine components. This yields 3 additional feature channels (1 magnitude and 2 phase). These seven feature channels are computed across 15 frequencies and 3 antennas at each time instant. To capture temporal information, we stack features over 3 consecutive timestamps, forming a spectrogram-like representation. Depending on the use case, we use either one or three antennas. For tasks that benefit from faster, more localized sensing, such as widget interaction (Section 6.3), we use a single antenna, yielding 315 features in total (7 channels × 15 frequencies × 3 timestamps). For tasks where spatial distribution is more informative, such as grip pose detection (Section 6.1), we use three antennas, yielding 945 features (7 channels × 15 frequencies × 3 timestamps × 3 antennas).

We implement the model in Python using the scikit-learn library [50, 51] and use the Extra Trees algorithm with 100 estimators. Depending on the task type, we use either classification or regression: most tasks are modeled with an ExtraTreesClassifier, while the slider and knob tasks use an ExtraTreesRegressor to predict continuous values. To improve stability, we apply a voting window over 5 consecutive predictions and display the most frequent predicted output. These prediction results are then used in real time by downstream applications, such as triggering shortcuts and interactive controls.

## 3.6 RF Field Characterization

To characterize the sensing range of our cellular antenna-impedance-based approach, we conducted an experiment that probes the smartphone's RF field. Our approach leverages the fact that nearby conductive (or dielectric) objects change the cellular antenna impedance, which in turn changes the antenna's measured reflection coefficient (S11). To examine how these changes vary over space, we prepared a wideband meandered monopole antenna (Figure 4, close-up), positioned at controlled locations near the smartphone, and recorded the resulting S11 changes from the smartphone. The probing antenna was tuned to cellular frequencies. It has a total length of 160 mm, with resonances measured by an external vector network analyzer at 917 MHz, 1901 MHz, and 2420 MHz. Defining bandwidth by the standard 3 dB criterion, the second and third resonances have bandwidths of 330 MHz and 245 MHz, respectively, which cover the cellular frequency bands used in our system (see Section 3.2).

The experimental apparatus is shown in Figure 4. We attached the monopole antenna to the tip of a computer numerical control (CNC) platform and scanned it at 5 mm intervals over a 140 × 215 mm area surrounding the smartphone, while maintaining the antenna at a height of 3 mm above the smartphone screen. We

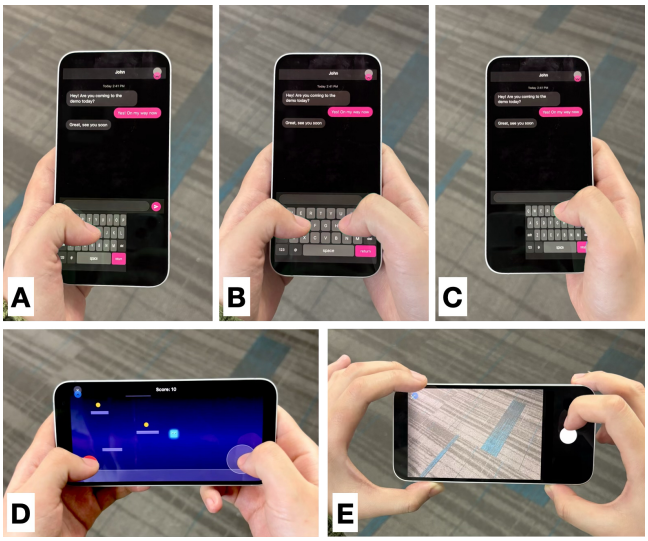



**Figure 6: Grip pose detection could allow for smartphones to automatically adjust the keyboard (A-C) or offer quick system-wide access to the camera (D→E).**




**Figure 7: One of two example interactive phone cases we made (see also Figure 9). Here, a camera-enthusiast case provides mechanical controls for exposure, zoom, and shutter. See Figure 13 for close-ups of example widget designs.**

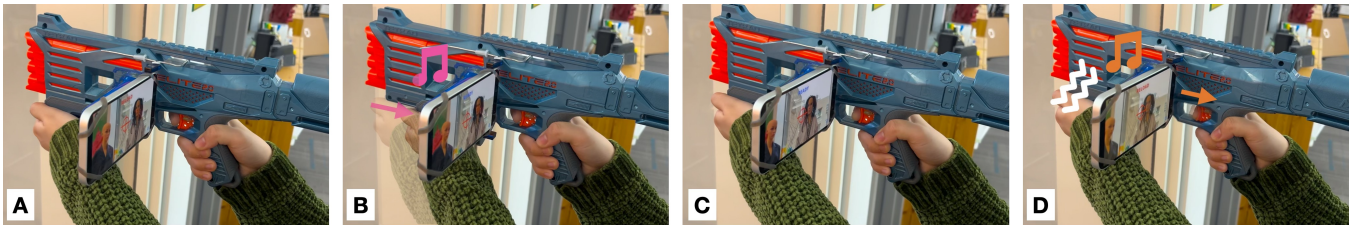



**Figure 8: A user docks their smartphone into an inexpensive, passive toy. The smartphone can sense the finger trigger and pump-action reload, augmenting the user experience with visuals, sound effects, and vibration. See Figure 13 for close-ups of example widget designs.**

first measured the baseline S11 values with no probing antenna nearby (i.e., probing antenna positioned 15 cm away from the smartphone edge). We then subtracted this reference value from the S11 measurements recorded when the probing antenna was moved to each location of interest. For this study, we used all three antennas (Figure 5, left) and seven bands (B1, B2, B3, B7, B30, B66, N25).

Importantly, we measured S11 changes directly on the smartphone rather than using external sensing hardware. The probing monopole antenna was untethered and mounted to the CNC machine through a non-conductive acrylic fixture to minimize extraneous electrical coupling. The RF sensing field is visualized as a heatmap in Figure 5. We observe that the sensing field is effective up to approximately 1.5–2 cm around the device, making it suitable for near-device interaction scenarios such as grip pose and surface material recognition.

## 4 Example Use Cases

As a proof of concept, we created five demo applications, which we also use as experimental probes to evaluate the efficacy of our approach (Section 5). Of important note, all five of these use cases have been previously demonstrated and validated in the literature. We purposefully reproduce this prior functionality to underscore how this sensing is possible using ubiquitous smartphones (vs. a variety of sensing methods, many of which are specialized for the task). This also permits us to roughly compare the accuracy between smartphone-based RF sensing and prior sensing methods.

### 4.1 Grip Pose Detection

Devices that can sense the grip pose of their owners could automatically launch applications, trigger functionality, or adapt their behaviors to improve user performance. For example, the camera app could launch automatically when the phone is held like a camera (Figure 6), an idea already explored in HandSee [77]. Additionally, the on-screen keyboard could adapt its behavior based on whether the user is typing with, e.g., two thumbs, either the left or right thumb, or other digits (information already shown to be advantageous in OmniSense [74]). To explore whether such sensing is possible with our approach, we curated a set of 8 hand poses drawn from prior work [23, 24, 78], shown in Figure 10 (and evaluated in Section 6.1).

### 4.2 Worn Placement Detection

Mobile devices that can infer where they are placed or held have been previously explored by Wiese et al. [62], RadarCat [73], and Botential [37]. With such knowledge, mobile devices could adapt their behaviors intelligently. For example, if a phone is in a pocket during an incoming call, it is effective to employ a haptic alert, but it is ineffective to turn on the screen. Conversely, if the device is resting on a table, turning on the screen and employing an audio alert will be more effective (and power-efficient) than employing haptics. As another example, a smartphone step counter could produce better estimates with knowledge of where the device is located on the user, as the kinematic signal changes based on device placement. As a proof-of-concept worn location test set, we selected held to head, in hand, in pocket (screen facing towards the body), in pocket (screen facing out), on lap, and off body (on table), seen in Figure 12. Note that cloth has very little mass, and so our signal is dominated by the user's body coupling and not articles of clothing when in the pocket.

### 4.3 Interactive Passive Cases

It is also possible to create small passive mechanical "widgets" that vary the shape or position of a small conductor, such that we can purposely alter a cellular antenna's response. Figure 13 provides four commonplace binary and analog widget examples: momentary

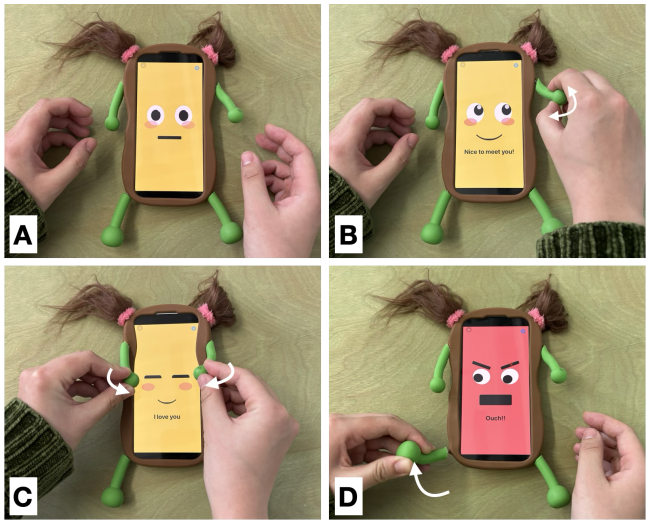



**Figure 9: One of two example interactive phone cases we created (see also Figure 7). Here, a child's smartphone lock screen is brought to life with an interactive avatar. See Figure 13 for close-ups of example widget designs.**

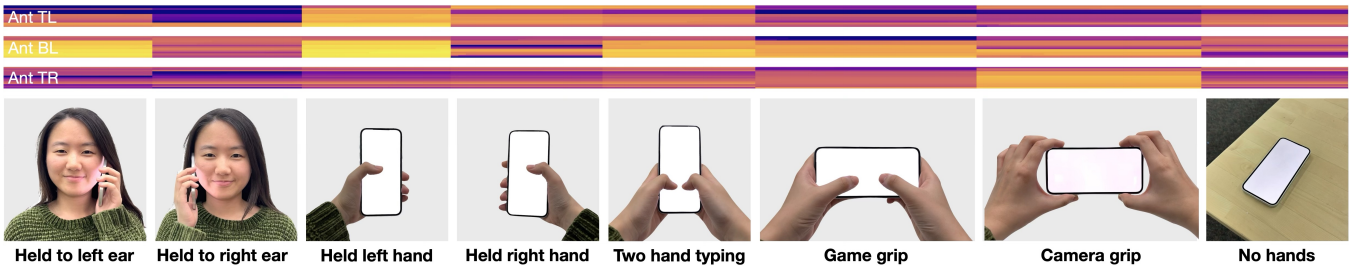



**Figure 10: Bottom: Example hand grips detectable with smartphone RF sensing. Top: magnitude spectrograms (1.7-2.6 GHz, 3 antennas) captured while a user performed each grip in sequence.**

button, toggle switch, linear slider, and turn knob. These mechanical widgets could be integrated into smartphone cases, offering tangible interactive functionality in a low-cost, battery-free manner. We created two example cases for illustration. First, we created a camera-enthusiast case, featuring a physical shutter button, a slider for zoom, and a turn knob for exposure (Figure 7). For a second example, we created a case for kids: the phone's lock screen features an avatar that responds to manipulations of limbs that extend from the case (Figure 9).

## 4.4 Plug-and-Play Accessories

We envision smartphones being docked into larger, low-cost, battery-free objects. The smartphone acts as a transient, plug-and-play "brain" with advanced interactive capabilities (graphics, sound, haptics, wireless communication, etc.). As one example of this idea, we instrumented a $10 foam dart gun toy with a phone holder and extended its plastic mechanisms with slider widgets (see previous section) such that the phone can sense the toy's pump action and finger trigger (Figure 8B). The phone provides a passthrough augmented reality experience with an overlaid crosshair and ammo counter, and generates sound effects and haptics when the user fires a dart (Figure 8D).

## 4.5 Surface Recognition

Surface detection is conceptually similar to worn placement detection and has been previously explored in work such as Harrison and Hudson [13]. We note that RadarCat [73] used radar for material sensing, an RF method, and takes advantage of similar phenomena to detect materials (chiefly density). A device that can sense its host surface's material could infer where it is placed, either on the body or in the greater environment. For instance, a device could learn the material of a user's bedside table and adapt its behavior accordingly (e.g., entering silent mode automatically based on placement rather than time of day; see Figure 11A). Other behaviors or apps could be triggered when placed on a user's kitchen countertop (e.g., the touchscreen could become more tolerant of wet fingers) or dining room table (e.g., do not disturb mode automatically engaged). If a smartphone is placed onto a laptop or tablet, it could trigger, e.g., the transfer of files (Figure 11B). As a representative material set for evaluation, we selected a wood table, medium-density fiberboard (MDF), faux leather sofa, fabric armchair, insulation foam, glass shelf, quartz countertop, ceramic tile, copper foil, stainless steel sheet, MacBook keyboard, iPad screen, and book (Figure 14).

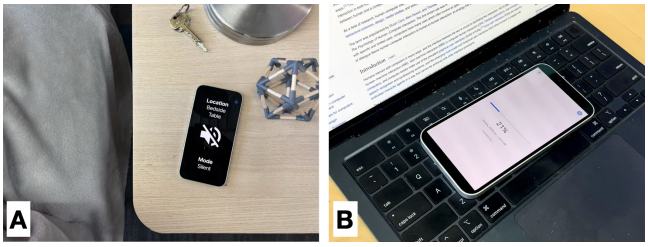



**Figure 11: Smartphones with surface recognition capabilities could automatically adjust their modes (e.g., go into silent mode whenever placed on the user's bedside table; A) or trigger contextual functionality (e.g., transmit a file to the user's laptop if placed on top; B).**

# 5 Evaluation

To evaluate the efficacy and generalizability of using smartphone RFFEs for sensing, we created a series of diverse study tasks derived from our example use cases (Section 4). For grip detection, we curated a set of 8 classes seen in Figure 10. For worn placement detection, we selected five locations seen in Figure 12. For material detection, we used the 13-class set seen in Figure 14. To represent the types of mechanisms that could be used in interactive passive cases and plug-and-play accessories, we selected four fundamental widgets, representing binary and analog actions (Figure 13).

## 5.1 Participants & Procedure

For all of our study tasks except surface detection, the user's proximate hand can influence the RF signal. Thus, we collected data in a

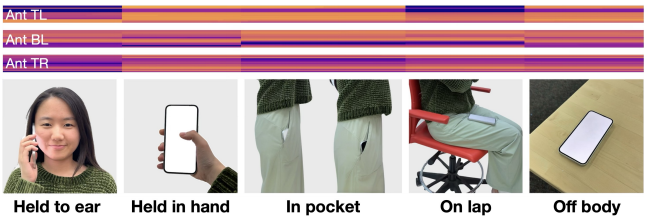



**Figure 12: Bottom: Example worn placements detectable with smartphone RF sensing, including two in-pocket subclasses: screen facing inward and outward. Top: magnitude spectrograms (1.7–2.6 GHz, 3 antennas) recorded as a user performed each placement in sequence.**

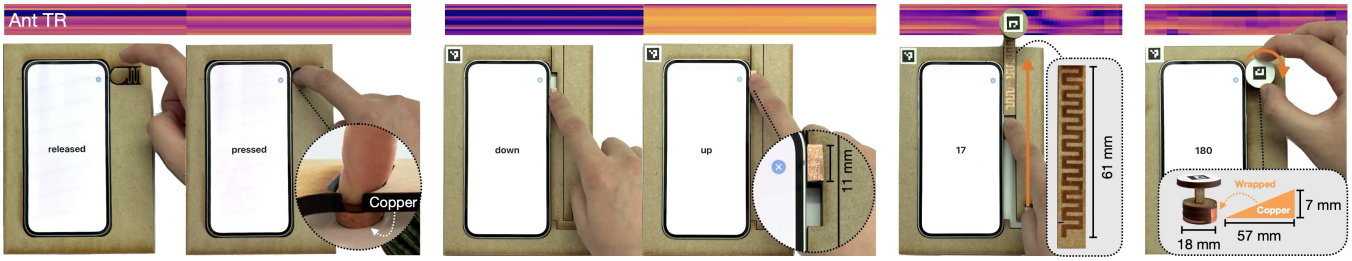



**Figure 13: Bottom: Passive widget examples we created for our user study. The slider had a maximum translation of 100 mm. The turn knob was continuous. Top: magnitude spectrograms (1.7-2.6 GHz; only antenna TR shown, which is next to the widget) captured while a user interacted with each mechanism. For the push and toggle buttons, one action is shown. For the slider, the user completes one full translation from bottom to top. For the turn knob, the user completes one full rotation.**

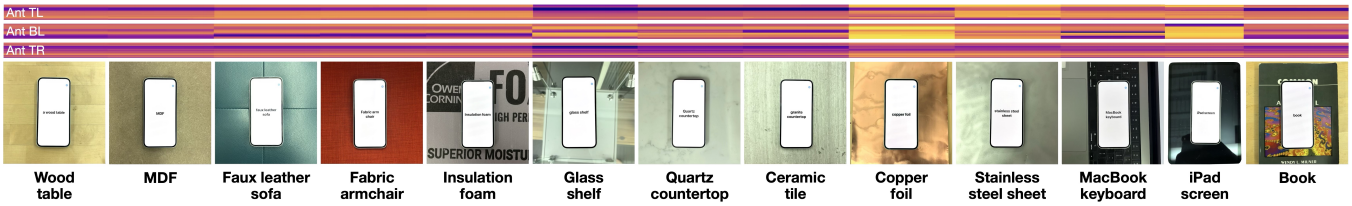



**Figure 14: Bottom: Example set of surface materials used in our evaluation. Top: magnitude spectrograms (1.7-2.6 GHz, 3 antennas) captured while a user placed the phone down onto each material in sequence.**

user study format to capture realistic influence from a proximate user. We recruited 12 participants (mean age 26.8 years, SD=2.8; 6 male, 5 female, and 1 non-binary) for this study, which lasted approximately 30 minutes and paid $10 USD in compensation.

***Grip Pose & Worn Placement Detection.*** Our grip detection and worn placement detection study tasks followed the same overall procedure. Participants were first familiarized with each study task's class set (Figures 10 and 12). After this, they were not corrected or constrained in how they performed the requested class, introducing natural variation. Participants were verbally instructed to switch to different classes, one at a time, in a random order, during which time 20 frames of data were collected with a ground truth label. One round of data consisted of each class appearing once, and each study task collected five rounds of data. Thus, for our grip detection study task, this meant that we captured 8 classes × 5 rounds × 20 frames of data × 12 participants = 9600 total grip data frames. Likewise, for worn placement detection, we collected 7200 total frames. Participants were told to wear clothes with pockets, but no other constraints were given; participants arrived with a mix of clothing fabrics. For the in-pocket class as part of worn placement detection, we collected equal trials of the screen facing towards the body and the screen facing outwards, combining the data into a single class. Participants were generally stationary during the experiments, though we did not explicitly constrain them.

***Widget Interaction (push & toggle buttons).*** To evaluate our widget mechanisms, we fabricated each passive widget using a small antenna and a wooden structure positioned near the top right cellular antenna (ANT TR) region. For the push button (Figure 13, left), we laser-cut a spring-like structure and wrapped copper tape around its side. For the toggle button (Figure 13, center), we inserted a small copper-wrapped block that mechanically moved to block or unblock the antenna region. For the push button, we recorded 20 frames of data with the button released and 20 frames of data with the button continuously pressed by the user. For the toggle switch, we had the user toggle it one way, followed by capture of 20 frames of data, and then toggle it the other way, followed by capture of 20 frames of data. The latter sequence is considered one round of data for our two binary widgets, and participants completed 5 rounds. Per widget, we collected 2400 frames (2 classes × 5 rounds × 20 frames of data × 12 participants).

***Widget Interaction (slider & turn knob).*** For the linear slider, we fabricated a movable meander antenna with an overall length of 60 mm (Figure 13, slider). For the turn knob, we wrapped a triangular copper patch around a cylindrical knob with a diameter of 18 mm (Figure 13, right). As both are analog widgets, we utilize a small printed ArUco marker and overhead webcam to record the ground truth value in real time, which we pair with live sensor data. ArUco marker accuracy is approximately 1 mm and 1° [32]. One round of data was captured per participant, where they incrementally (~4 mm) translated the slider position until it reached 100 mm. Likewise, for the turn knob, the user incrementally rotated (~15°) the knob clockwise to complete a rotation. In total, we collected 6120 frames of slider movement and 4520 frames of knob movement.

***Surface Recognition.*** To evaluate surface recognition, we did not recruit participants; instead, one of the authors placed the device on each surface and withdrew their hand. During data collection, the surface label for the current trial was presented in randomized order within the surface group, and this process was repeated for 10 rounds. The device placement and orientation on each surface were varied so that each trial represented a unique configuration. We collected 20 frames of data for each surface trial, which yielded 2600 frames (13 surfaces × 10 rounds × 20 frames) for evaluation.

## 5.2 Train-Test Procedure

We evaluate model performance using three validation schemes. First, we use leave-one-round-out cross-validation, where data from one recording round from a single participant is held out for testing, and all other remaining rounds are used for training. This results in 10 folds for the surface recognition task and 60 folds for all other study tasks. Second, we also use leave-one-participant-out cross-validation, where all data from one participant is held out for testing, and the model is trained on data from the remaining eleven participants, resulting in 12 folds. Third, we use a 60:40 data split scheme, i.e., 60% of the data for training and the remaining 40% of the data for testing, while within-session data are not mixed between train and test. For reporting accuracy and error, we average the results across all cross-validation folds.

# 6 Results & Discussion

Figure 15 summarizes our main results. Overall, co-opting mobile cellular antennas enables a diverse range of applications with above 90% accuracy on tasks that previously required specialized sensing.

## 6.1 Grip Pose Detection

With our leave-one-round-out train-test procedure, we found a mean grip pose detection accuracy of 91.3% (SD=9.9). The confusion matrix is shown in Figure 16. Note that the previous model contains some training data from the participant being tested, though it never mixes data within sessions. A more conservative estimate of accuracy is a leave-one-participant-out test scheme, where no data from the user being tested is in the training set (simulating a general model, without user calibration). With this train-test setup, we find an accuracy of 81.1% (SD=12.2). Under a 60:40 data split scheme, the performance shows 91.6% detection accuracy. We observed individual differences in how participants grasped the phone. For example, regarding the held-to-ear pose, some participants touched their skin to the screen, whereas others held it away from their head. This may explain the confusion between held-to-ear and held-hand poses. In addition, our system does not include an antenna at the bottom-right of the device, reducing spatial resolution in that region. This is likely why there was confusion between two-hand typing and held-left-hand.

Our results are competitive with prior smartphone grip-sensing work. For example, SmartGrip [24] was able to demonstrate 93.1% accuracy with a six-class grip pose set using smartphone-emitted ultrasound. GripSense [9] classifies three in-hand postures with an accuracy of 84.3% using built-in sensors, including accelerometer, gyroscope, and touchscreen. ReflecTouch [78] uses a front-facing camera to image the screen reflection in the cornea, showing 85% for the six-posture classification task. Kim et al. [23] use an external capacitive sensor array under the phone's exterior cover and show 91.8% of the best cross-validation accuracy over eight grip patterns. Overall, our results demonstrate comparable performance while supporting a larger set of grip classes using sensors already available in modern mobile devices.

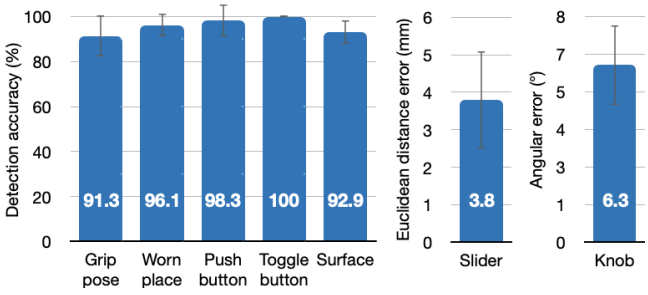



**Figure 15: Accuracy summary for our five classification and two regression study results.**

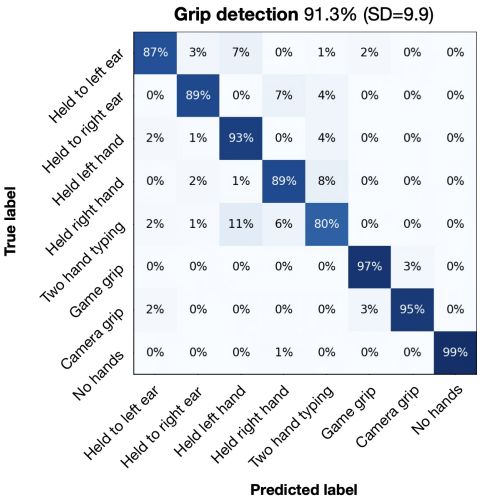



**Figure 16: Grip pose detection confusion matrix.**

## 6.2 Worn Placement Detection

Detection accuracy is 96.6% (SD=8.8) in leave-one-round-out, 93.4% (SD=11.4) in leave-one-participant-out, and 96.0% in 60:40 train-to-test split schemes. The confusion matrix for each class is shown in Figure 17. As noted earlier in the grip pose detection results, we observed individual differences in how users held the device to their ear, with some holding it close to the head and others farther away. This likely explains the misclassification between held to ear and held in hand, as a phone held farther from the head can appear similar to a regular hand-held pose.

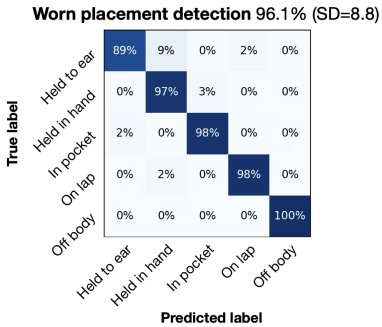



**Figure 17: Worn-placement detection Confusion matrix.**

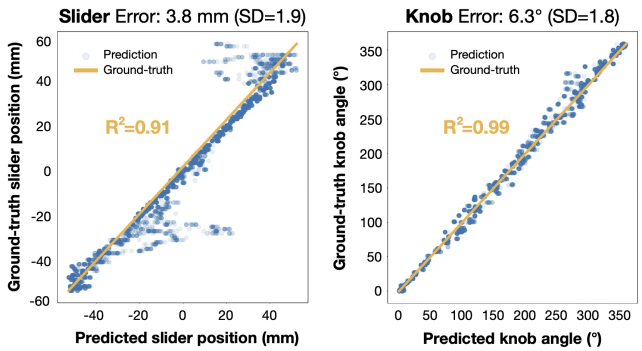



**Figure 18: Scatter plots of predicted vs. ground truth values for slider position and turn knob angle. See also Figure 13.**

For comparison, Yang et al. [71] classify three phone placements (in-pocket, in-bag, neither) using proximity and light sensors, and achieved an accuracy of 98%. Phoneprioception [62] shows 75.4% accuracy on four classes, including the classes mentioned in [71] plus the in-hand class. GripSense [9] reported 99.7% accuracy for a binary in-hand vs. flat-surface classification using a phone's vibration motor and IMU. Compared with these prior works, our method shows similarly high performance across a larger range of classes.

## 6.3 Widget Interaction

The binary push and toggle buttons achieved classification accuracies of 98.3% (SD=8.0) and 100.0% (SD=0), respectively. For the analog widgets, the slider yielded a mean prediction error of 3.8 mm (SD=1.9), while the turn knob yielded a mean angular error of 6.3° (SD=1.8). Figure 18 plots the predicted values against the ground-truth values for all test samples, where the diagonal line indicates perfect agreement and deviations from this line represent prediction error. The corresponding coefficients of determination ($R^2$) are 0.91 for the slider and 0.99 for the turn knob.

Many prior systems have explored near-smartphone widgets using modalities such as acoustics [28, 49, 56, 66], magnetics [18, 34, 35, 76], and other embedded sensing approaches. Many of these works evaluate the system primarily through implementation and demonstrations rather than directly comparable accuracy or physical-error metrics. Among the closest comparisons, Acoustruments [28] reported 99.5% button recognition accuracy (SD=0.07) and a mean knob error of 7.8° (SD=6.0). Lamello [49] achieves 93% precision for the discrete four-tine slider. TRing [76] demonstrates 4.96 mm of 2D tracking error for a finger-worn magnet near the magnetometer. Relative to this set of prior work, our widgets achieve comparable performance and fine-grained analog inputs.

## 6.4 Surface Recognition

Across 13 surface materials, the detection accuracy was 92.9% (SD = 5.5) in the leave-one-round-out scheme and 99.9% in the 60:40 train-to-test split scheme. The confusion matrix is shown in Figure 19. Most misclassifications occurred among the wood table, medium-density fiberboard (MDF), and book classes, likely because these materials share similar structural properties despite differences in

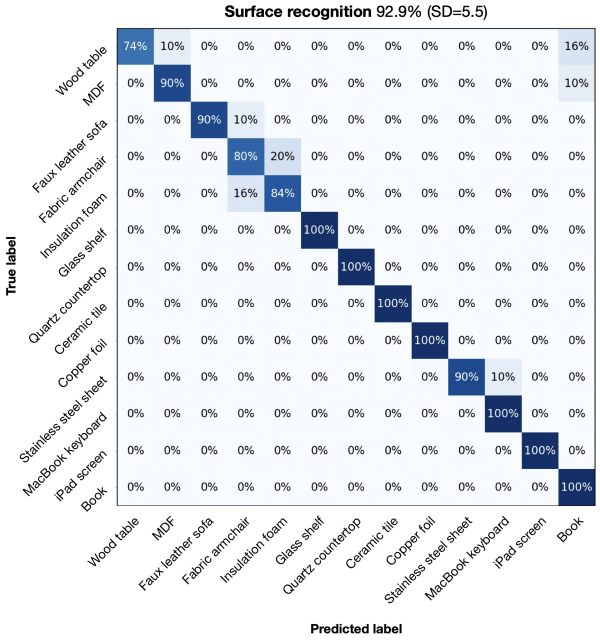



**Figure 19: Surface recognition confusion matrix.**

density, though our RF-based approach still achieved accuracies of at least 74% for these classes. We also observed confusion between the fabric armchair and insulation foam classes, which is explained by their similar composition.

In comparison to prior work, SurfaceSense [6] reported 91.75% recognition accuracy over 13 different surfaces using a two-tier placement-aware approach using multiple built-in sensors, including accelerometer, gyroscope, magnetometer, microphone, and proximity sensor. RadarCat [73] reported 98.67% accuracy (SD=0.9) over 26 surfaces and objects using a 60 GHz radar sensor. While RadarCat achieves higher accuracy, it relies on specialized high-frequency radar hardware, which likely provides greater material sensitivity than our cellular-band sensing approach. In contrast, our method achieves comparable performance using only the cellular antenna already built into a commercial smartphone.

## 6.5 Automatic Model-Switching

While the previous sections describe task-specific models, a practical deployment of our system would require a pipeline to automatically activate the appropriate model based on the user's current context. To achieve this, we trained a mode-switching model that classifies the device state into three primary contexts: in-hand, on-body, or off-body. Using aggregated data from our Grip Pose, Worn Placement, and Surface Recognition studies, this three-class classifier achieved 99.7% accuracy with a 60:40 train-test split (11,980 training : 8,060 testing samples). Additionally, explicit user actions (e.g., launching an AR toy app in Figure 8) can directly activate application-specific models.

# 7 Limitations & Future Work

A limitation precluding some use cases is sensing range. Our field characterization shows that the effect is largely confined to the

immediate volume around the phone, with useful sensitivity extending only roughly 2 cm from the device. This makes the approach well suited to near-device interactions (e.g., grip sensing, passive widgets, surface recognition), but it also means that longer-range interaction scenarios appear infeasible with the present hardware and frequency range. Future work could investigate whether other antennas already present in mobile devices, alternative bands, or fused multimodal sensing could extend the practical interaction volume beyond the handset's immediate vicinity.

Next, our sensing framerate is constrained by hardware originally designed for communication rather than measurement. Although the RFFE allows us to sample densely within each cellular band, we only measure three points to maintain interactive performance (0.4 FPS when capturing a full frame of data). However, this is sufficient for proof-of-concept demonstrations involving relatively stable states, such as held pose, worn placement, and surface recognition. That said, we believe this bottleneck to be largely a function of our current measurement sequencing approach rather than a fundamental limitation of the underlying hardware.

Our system may incur additional energy consumption due to increased polling of RFFE data and, in some configurations, more frequent antenna tuning or measurements across multiple cellular bands. However, these operations leverage hardware and feedback mechanisms that are already optimized for power efficiency. We therefore expect the incremental energy overhead to be modest, although a comprehensive characterization of power consumption across devices and usage patterns remains an important direction for future work.

Our current implementation temporarily assumes control of the RFFE, preventing concurrent use of the cellular radio for communication. This reflects a limitation of our prototype, not of the underlying hardware. Because modern modems already coordinate antenna tuning, power tracking, and band selection as part of normal operation, future commercial implementations could integrate RF sensing directly into these existing control loops. Such integration may allow communication and sensing to coexist, for example by scheduling sensing measurements during normal radio operation or opportunistically utilizing measurements already collected by the modem.

Overall, we believe our underlying sensing approach is broadly applicable to modern mobile platforms. Dynamic antenna tuning, power monitoring, and adaptive impedance matching are fundamental capabilities required to support contemporary 4G LTE and 5G radios operating across numerous frequency bands within the constrained form factors of smartphones. While the specific APIs and implementation details may differ among vendors, the underlying hardware mechanisms that enable our approach are likely common to most modern smartphones and, increasingly, other cellular-enabled devices such as smartwatches and tablets.

Overall, while our results show that smartphone RFFE sensing is promising and can be generalized to several existing HCI use cases, they should be interpreted as an existence proof rather than a complete characterization of the method. Future work is needed to study cross-device generalization, impact of protective cases, robustness across environments and users, long-term stability, and how RF sensing can be combined with other on-device sensors to support richer and more reliable interactive systems.

# 8 Conclusion

The main finding of our work is that modern smartphones contain latent RF measurement capabilities that, when accessed through the cellular modem subsystem, function as embedded and software-defined RF sensing instruments. This perspective transforms communication subsystems into opportunistic sensing platforms, enabling new avenues of human–device interaction that leverage electromagnetic coupling as an input modality.

# References


[1] Fadel Adib, Hongzi Mao, Zachary Kabelac, Dina Katabi, and Robert C. Miller. 2015. Smart Homes that Monitor Breathing and Heart Rate. In *Proceedings of the 33rd Annual ACM Conference on Human Factors in Computing Systems* (Seoul, Republic of Korea) *(CHI '15)*. Association for Computing Machinery, New York, NY, USA, 837–846. doi:10.1145/2702123.2702200

[2] Marwa AlAlawi, Regina Zheng, Sooyeon Ahn, Katherine Yan, Ticha Sethapakdi, Junyi Zhu, and Stefanie Mueller. 2025. Meta-antenna: Mechanically Frequency Reconfigurable Metamaterial Antennas. In *Proceedings of the 38th Annual ACM Symposium on User Interface Software and Technology (UIST '25)*. Association for Computing Machinery, New York, NY, USA, Article 36, 19 pages. doi:10.1145/3746059.3747760

[3] Alex Butler, Shahram Izadi, and Steve Hodges. 2008. SideSight: multi-"touch" interaction around small devices. In *Proceedings of the 21st Annual ACM Symposium on User Interface Software and Technology* (Monterey, CA, USA) *(UIST '08)*. Association for Computing Machinery, New York, NY, USA, 201–204. doi:10.1145/1449715.1449746

[4] Le Chang, Zhijun Zhang, and Magdy F. Iskander. 2024. *Mobile Antenna History Between 1983 and 2022*. Springer International Publishing, Cham, 385–418. doi:10.1007/978-3-031-39824-7_14

[5] Xiang 'Anthony' Chen, Julia Schwarz, Chris Harrison, Jennifer Mankoff, and Scott E. Hudson. 2014. Air+touch: interweaving touch & in-air gestures. In *Proceedings of the 27th Annual ACM Symposium on User Interface Software and Technology* (Honolulu, Hawaii, USA) *(UIST '14)*. Association for Computing Machinery, New York, NY, USA, 519–525. doi:10.1145/2642918.2647392

[6] Rajkumar Darbar and Debasis Samanta. 2015. SurfaceSense: Smartphone Can Recognize Where It Is Kept. In *Proceedings of the 7th Indian Conference on Human-Computer Interaction* (Guwahati, India) *(IndiaHCI '15)*. Association for Computing Machinery, New York, NY, USA, 39–46. doi:10.1145/2835966.2835971

[7] Electronic Engineering Times China. 2023. *A Detailed Discussion of the Development of Smartphone Antennas*. https://www.eet-china.com/mp/a274693.html

[8] FrequencyCheck. 2026. Samsung SM-S938B Galaxy S25 Ultra 5G Global TD-LTE 1TB - Frequency Bands and Network Compatibility. https://www.frequencycheck.com/models/GBkoz/samsung-sm-s938b-galaxy-s25-ultra-5g-global-td-lte-1tb-samsung-paradigm-3. Accessed: 2026-03-12.

[9] Mayank Goel, Jacob Wobbrock, and Shwetak Patel. 2012. GripSense: using built-in sensors to detect hand posture and pressure on commodity mobile phones. In *Proceedings of the 25th Annual ACM Symposium on User Interface Software and Technology* (Cambridge, Massachusetts, USA) *(UIST '12)*. Association for Computing Machinery, New York, NY, USA, 545–554. doi:10.1145/2380116.2380184

[10] Anhong Guo, Robert Xiao, and Chris Harrison. 2015. CapAuth: Identifying and Differentiating User Handprints on Commodity Capacitive Touchscreens. In *Proceedings of the 2015 International Conference on Interactive Tabletops & Surfaces* (Madeira, Portugal) *(ITS '15)*. Association for Computing Machinery, New York, NY, USA, 59–62. doi:10.1145/2817721.2817722

[11] Sidhant Gupta, Daniel Morris, Shwetak Patel, and Desney Tan. 2012. SoundWave: using the doppler effect to sense gestures. In *Proceedings of the SIGCHI Conference on Human Factors in Computing Systems* (Austin, Texas, USA) *(CHI '12)*. Association for Computing Machinery, New York, NY, USA, 1911–1914. doi:10.1145/2207676.2208331

[12] Teng Han, Khalad Hasan, Keisuke Nakamura, Randy Gomez, and Pourang Irani. 2017. SoundCraft: Enabling Spatial Interactions on Smartwatches using Hand Generated Acoustics. In *Proceedings of the 30th Annual ACM Symposium on User Interface Software and Technology* (Québec City, QC, Canada) *(UIST '17)*. Association for Computing Machinery, New York, NY, USA, 579–591. doi:10.1145/3126594.3126612

[13] Chris Harrison and Scott E. Hudson. 2008. Lightweight material detection for placement-aware mobile computing. In *Proceedings of the 21st Annual ACM Symposium on User Interface Software and Technology* (Monterey, CA, USA) *(UIST '08)*. Association for Computing Machinery, New York, NY, USA, 279–282. doi:10.1145/1449715.1449761

[14] Chris Harrison and Scott E. Hudson. 2009. Abracadabra: wireless, high-precision, and unpowered finger input for very small mobile devices. In *Proceedings of the 22nd Annual ACM Symposium on User Interface Software and Technology* (Victoria, BC, Canada) *(UIST '09)*. Association for Computing Machinery, New York, NY,

USA, 121–124. doi:10.1145/1622176.1622199

[15] Ken Hinckley, Seongkook Heo, Michel Pahud, Christian Holz, Hrvoje Benko, Abigail Sellen, Richard Banks, Kenton O'Hara, Gavin Smyth, and William Buxton. 2016. Pre-Touch Sensing for Mobile Interaction. In *Proceedings of the 2016 CHI Conference on Human Factors in Computing Systems* (San Jose, California, USA) *(CHI '16)*. Association for Computing Machinery, New York, NY, USA, 2869–2881. doi:10.1145/2858036.2858095

[16] Christian Holz, Senaka Buthpitiya, and Marius Knaust. 2015. Bodyprint: Biometric User Identification on Mobile Devices Using the Capacitive Touchscreen to Scan Body Parts. In *Proceedings of the 33rd Annual ACM Conference on Human Factors in Computing Systems* (Seoul, Republic of Korea) *(CHI '15)*. Association for Computing Machinery, New York, NY, USA, 3011–3014. doi:10.1145/2702123.2702518

[17] Wonbin Hong. 2017. Solving the 5G Mobile Antenna Puzzle: Assessing Future Directions for the 5G Mobile Antenna Paradigm Shift. *IEEE Microwave Magazine* 18, 7 (2017), 86–102. doi:10.1109/MMM.2017.2740538

[18] Sungjae Hwang, Myungwook Ahn, and Kwang-yun Wohn. 2013. MagGetz: customizable passive tangible controllers on and around conventional mobile devices. In *Proceedings of the 26th Annual ACM Symposium on User Interface Software and Technology* (St. Andrews, Scotland, United Kingdom) *(UIST '13)*. Association for Computing Machinery, New York, NY, USA, 411–416. doi:10.1145/2501988.2501991

[19] Sungjae Hwang, Andrea Bianchi, Myungwook Ahn, and Kwangyun Wohn. 2013. MagPen: magnetically driven pen interactions on and around conventional smartphones. In *Proceedings of the 15th International Conference on Human-Computer Interaction with Mobile Devices and Services* (Munich, Germany) *(MobileHCI '13)*. Association for Computing Machinery, New York, NY, USA, 412–415. doi:10.1145/2493190.2493194

[20] Daehwa Kim and Chris Harrison. 2022. EtherPose: Continuous Hand Pose Tracking with Wrist-Worn Antenna Impedance Characteristic Sensing. In *Proceedings of the 35th Annual ACM Symposium on User Interface Software and Technology* (Bend, OR, USA) *(UIST '22)*. Association for Computing Machinery, New York, NY, USA, Article 58, 12 pages. doi:10.1145/3526113.3545665

[21] Daehwa Kim and Chris Harrison. 2023. pantoenna: Mouth pose estimation for ar/vr headsets using low-profile antenna and impedance characteristic sensing. In *Proceedings of the 36th Annual ACM Symposium on User Interface Software and Technology* (San Francisco, CA, USA) *(UIST '23)*. Association for Computing Machinery, New York, NY, USA, Article 83, 12 pages. doi:10.1145/3586183.3606805

[22] Daehwa Kim, Keunwoo Park, and Geehyuk Lee. 2021. AtaTouch: Robust Finger Pinch Detection for a VR Controller Using RF Return Loss. In *Proceedings of the 2021 CHI Conference on Human Factors in Computing Systems* (Yokohama, Japan) *(CHI '21)*. Association for Computing Machinery, New York, NY, USA, Article 11, 9 pages. doi:10.1145/3411764.3445442

[23] Kee-Eung Kim, Wook Chang, Sung-Jung Cho, Junghyun Shim, Hyunjeong Lee, Joonah Park, Youngbeom Lee, Sangryoung Kim, et al. 2006. Hand grip pattern recognition for mobile user interfaces. In *Proceedings of the National Conference on Artificial Intelligence*, Vol. 21. AAAI Press, 1789.

[24] Namhyun Kim, Junseong Lee, Joyce Jiyoung Whang, and Jinkyu Lee. 2020. SmartGrip: grip sensing system for commodity mobile devices through sound signals. *Personal and Ubiquitous Computing* 24, 5 (2020), 643–654.

[25] Seungki Kim, Jiwoo Hong, Jaeyeon Lee, Hyun-Sook Choi, Geehyuk Lee, and Woohun Lee. 2018. TouchBranch: Understanding Interpersonal Touches in Interactive Installation. In *Proceedings of the 2018 Designing Interactive Systems Conference* (Hong Kong, China) *(DIS '18)*. Association for Computing Machinery, New York, NY, USA, 535–546. doi:10.1145/3196709.3196740

[26] Andy Kong, Daehwa Kim, and Chris Harrison. 2024. Power-over-Skin: Full-Body Wearables Powered By Intra-Body RF Energy. In *Proceedings of the 37th Annual ACM Symposium on User Interface Software and Technology* (Pittsburgh, PA, USA) *(UIST '24)*. Association for Computing Machinery, New York, NY, USA, Article 3, 13 pages. doi:10.1145/3654777.3676394

[27] Sven Kratz and Michael Rohs. 2009. HoverFlow: expanding the design space of around-device interaction. In *Proceedings of the 11th International Conference on Human-Computer Interaction with Mobile Devices and Services* (Bonn, Germany) *(MobileHCI '09)*. Association for Computing Machinery, New York, NY, USA, Article 4, 8 pages. doi:10.1145/1613858.1613864

[28] Gierad Laput, Eric Brockmeyer, Scott E. Hudson, and Chris Harrison. 2015. Acoustruments: Passive, Acoustically-Driven, Interactive Controls for Handheld Devices. In *Proceedings of the 33rd Annual ACM Conference on Human Factors in Computing Systems* (Seoul, Republic of Korea) *(CHI '15)*. Association for Computing Machinery, New York, NY, USA, 2161–2170. doi:10.1145/2702123.2702414

[29] Gierad Laput, Robert Xiao, Xiang 'Anthony' Chen, Scott E. Hudson, and Chris Harrison. 2014. Skin buttons: cheap, small, low-powered and clickable fixed-icon laser projectors. In *Proceedings of the 27th Annual ACM Symposium on User Interface Software and Technology* (Honolulu, Hawaii, USA) *(UIST '14)*. Association for Computing Machinery, New York, NY, USA, 389–394. doi:10.1145/2642918.2647356

[30] Gierad Laput, Robert Xiao, and Chris Harrison. 2016. ViBand: High-Fidelity Bio-Acoustic Sensing Using Commodity Smartwatch Accelerometers. In *Proceedings of the 29th Annual Symposium on User Interface Software and Technology* (Tokyo, Japan) *(UIST '16)*. Association for Computing Machinery, New York, NY, USA, 321–333. doi:10.1145/2984511.2984582

[31] Mathieu Le Goc, Stuart Taylor, Shahram Izadi, and Cem Keskin. 2014. A low-cost transparent electric field sensor for 3d interaction on mobile devices. In *Proceedings of the SIGCHI Conference on Human Factors in Computing Systems* (Toronto, Ontario, Canada) *(CHI '14)*. Association for Computing Machinery, New York, NY, USA, 3167–3170. doi:10.1145/2556288.2557331

[32] Vicente J León-Muñoz, Fernando Santonja-Medina, Francisco Lajara-Marco, Alonso J Lisón-Almagro, Jesús Jiménez-Olivares, Carmelo Marín-Martínez, Salvador Amor-Jiménez, Elena Galián-Muñoz, Mirian López-López, and Joaquín Moya-Angeler. 2023. The accuracy and absolute reliability of a knee surgery assistance system based on ArUco-type sensors. *Sensors* 23, 19 (2023), 8091.

[33] Yang Li and Youngwook Kim. 2017. Classification of Human Activities Using Variation in Impedance of Single On-Body Antenna. *IEEE Antennas and Wireless Propagation Letters* 16 (2017), 541–544. doi:10.1109/LAWP.2016.2588400

[34] Rong-Hao Liang, Liwei Chan, Hung-Yu Tseng, Han-Chih Kuo, Da-Yuan Huang, De-Nian Yang, and Bing-Yu Chen. 2014. GaussBricks: magnetic building blocks for constructive tangible interactions on portable displays. In *Proceedings of the SIGCHI Conference on Human Factors in Computing Systems* (Toronto, Ontario, Canada) *(CHI '14)*. Association for Computing Machinery, New York, NY, USA, 3153–3162. doi:10.1145/2556288.2557105

[35] Rong-Hao Liang, Kai-Yin Cheng, Liwei Chan, Chuan-Xhyuan Peng, Mike Y. Chen, Rung-Huei Liang, De-Nian Yang, and Bing-Yu Chen. 2013. GaussBits: magnetic tangible bits for portable and occlusion-free near-surface interactions. In *Proceedings of the SIGCHI Conference on Human Factors in Computing Systems* (Paris, France) *(CHI '13)*. Association for Computing Machinery, New York, NY, USA, 1391–1400. doi:10.1145/2470654.2466185

[36] Jaime Lien, Nicholas Gillian, M. Emre Karagozler, Patrick Amihood, Carsten Schwesig, Erik Olson, Hakim Raja, and Ivan Poupyrev. 2016. Soli: ubiquitous gesture sensing with millimeter wave radar. *ACM Trans. Graph.* 35, 4, Article 142 (July 2016), 19 pages. doi:10.1145/2897824.2925953

[37] Denys J. C. Matthies, Simon T. Perrault, Bodo Urban, and Shengdong Zhao. 2015. Botential: Localizing On-Body Gestures by Measuring Electrical Signatures on the Human Skin. In *Proceedings of the 17th International Conference on Human-Computer Interaction with Mobile Devices and Services* (Copenhagen, Denmark) *(MobileHCI '15)*. Association for Computing Machinery, New York, NY, USA, 207–216. doi:10.1145/2785830.2785859

[38] Rajalakshmi Nandakumar, Vikram Iyer, Desney Tan, and Shyamnath Gollakota. 2016. FingerIO: Using Active Sonar for Fine-Grained Finger Tracking. In *Proceedings of the 2016 CHI Conference on Human Factors in Computing Systems* (San Jose, California, USA) *(CHI '16)*. Association for Computing Machinery, New York, NY, USA, 1515–1525. doi:10.1145/2858036.2858580

[39] Joseph Paradiso and Kai Yuh Hsiao. 1999. Swept-frequency, magnetically-coupled resonant tags for realtime, continuous, multiparameter control. In *CHI '99 Extended Abstracts on Human Factors in Computing Systems* (Pittsburgh, Pennsylvania) *(CHI EA '99)*. Association for Computing Machinery, New York, NY, USA, 212–213. doi:10.1145/632716.632848

[40] Keunwoo Park, Daehwa Kim, Seongkook Heo, and Geehyuk Lee. 2020. MagTouch: Robust Finger Identification for a Smartwatch Using a Magnet Ring and a Built-in Magnetometer. In *Proceedings of the 2020 CHI Conference on Human Factors in Computing Systems* (Honolulu, HI, USA) *(CHI '20)*. Association for Computing Machinery, New York, NY, USA, 1–13. doi:10.1145/3313831.3376234

[41] Ivan Poupyrev, Zhiquan Yeo, Joshua D. Griffin, and Scott Hudson. 2010. Sensing human activities with resonant tuning. In *CHI '10 Extended Abstracts on Human Factors in Computing Systems* (Atlanta, Georgia, USA) *(CHI EA '10)*. Association for Computing Machinery, New York, NY, USA, 4135–4140. doi:10.1145/1753846.1754115

[42] Qifan Pu, Sidhant Gupta, Shyamnath Gollakota, and Shwetak Patel. 2013. Whole-home gesture recognition using wireless signals. In *Proceedings of the 19th Annual International Conference on Mobile Computing & Networking* (Miami, Florida, USA) *(MobiCom '13)*. Association for Computing Machinery, New York, NY, USA, 27–38. doi:10.1145/2500423.2500436

[43] Qorvo. 2019. Overcoming the RF Challenges of Full-Screen Smartphones. https://www.qorvo.com/resources/d/overcoming-the-rf-challenges-of-full-screen-smartphones-qorvo-white-paper Public white paper.

[44] Qualcomm, Inc. 2014. Next Generation Qualcomm RF360TM Front End Solution - QFE33xx CMOS PA, QFE10xx Antenna Switch, and QFE25xx Antenna Tuner simplify LTE-A RF complexity. http://www.qualcomm.com/content/dam/qcomm-martech/dm-assets/documents/rf360_gen_2_product_brief_rd8.2.pdf

[45] Qualcomm, Inc. 2016. Snapdragon™ 820 - LTE and Connectivity. Product brief. https://www.qualcomm.com/content/dam/qcomm-martech/dm-assets/documents/singapore_media_day_snapdragon-820-lte_and_connectivity_update-final_31-mar-2016.pdf (see slide 25).

[46] Maryam Sajedin, I.T.E. Elfergani, Jonathan Rodriguez, Raed Abd-Alhameed, and Monica Fernandez Barciela. 2019. A Survey on RF and Microwave Doherty Power Amplifier for Mobile Handset Applications. *Electronics* 8, 6 (2019). doi:10.3390/electronics8060717

[47] Samsung Electronics Co Ltd. 2024. Antenna gain_Main Band_240322. FCC test report for Samsung SMM356B, FCC ID A3LSMM356B. https://fcc.report/FCC-ID/A3LSMM356B/7196879

[48] Munehiko Sato, Ivan Poupyrev, and Chris Harrison. 2012. Touché: enhancing touch interaction on humans, screens, liquids, and everyday objects. In *Proceedings of the SIGCHI Conference on Human Factors in Computing Systems* (Austin, Texas, USA) *(CHI '12)*. Association for Computing Machinery, New York, NY, USA, 483–492. doi:10.1145/2207676.2207743

[49] Valkyrie Savage, Andrew Head, Björn Hartmann, Dan B. Goldman, Gautham Mysore, and Wilmot Li. 2015. Lamello: Passive Acoustic Sensing for Tangible Input Components. In *Proceedings of the 33rd Annual ACM Conference on Human Factors in Computing Systems* (Seoul, Republic of Korea) *(CHI '15)*. Association for Computing Machinery, New York, NY, USA, 1277–1280. doi:10.1145/2702123.2702207

[50] scikit-learn developers. 2026. *ExtraTreesClassifier*. https://scikit-learn.org/stable/modules/generated/sklearn.ensemble.ExtraTreesClassifier.html scikit-learn 1.8.0 documentation, accessed March 23, 2026.

[51] scikit-learn developers. 2026. *ExtraTreesRegressor*. https://scikit-learn.org/stable/modules/generated/sklearn.ensemble.ExtraTreesRegressor.html scikit-learn 1.8.0 documentation, accessed March 23, 2026.

[52] Semiconductor Today. 2017. Qualcomm launches RF front-end platform for next-generation global mobile devices. Magazine article. https://www.semiconductor-today.com/news_items/backissues/semiconductor-today-feb-2017.pdf Page 11.

[53] Skyworks Solutions, Inc. 2019. Mobile Antenna Solutions. Brochure. https://www.skyworksinc.com/-/media/SkyWorks/Documents/Brochures/Mobile-Antenna-Solutions.pdf

[54] Shunta Suzuki, Takashi Amesaka, Hiroki Watanabe, Buntarou Shizuki, and Yuta Sugiura. 2024. EarHover: Mid-Air Gesture Recognition for Hearables Using Sound Leakage Signals. In *Proceedings of the 37th Annual ACM Symposium on User Interface Software and Technology* (Pittsburgh, PA, USA) *(UIST '24)*. Association for Computing Machinery, New York, NY, USA, Article 129, 13 pages. doi:10.1145/3654777.3676367

[55] Ryo Takahashi, Eric Whitmire, Roger Boldu, Shiu Ng, Wolf Kienzle, and Hrvoje Benko. 2024. picoRing: battery-free rings for subtle thumb-to-index input. In *Proceedings of the 37th Annual ACM Symposium on User Interface Software and Technology* (Pittsburgh, PA, USA) *(UIST '24)*. Association for Computing Machinery, New York, NY, USA, Article 13, 11 pages. doi:10.1145/3654777.3676365

[56] Aaron Visschedijk, Hyunyoung Kim, Carlos Tejada, and Daniel Ashbrook. 2022. ClipWidgets: 3D-printed Modular Tangible UI Extensions for Smartphones. In *Proceedings of the Sixteenth International Conference on Tangible, Embedded, and Embodied Interaction* (Daejeon, Republic of Korea) *(TEI '22)*. Association for Computing Machinery, New York, NY, USA, Article 8, 11 pages. doi:10.1145/3490149.3501314

[57] Anandghan Waghmare, Youssef Ben Taleb, Ishan Chatterjee, Arjun Narendra, and Shwetak Patel. 2023. Z-Ring: Single-Point Bio-Impedance Sensing for Gesture, Touch, Object and User Recognition. In *Proceedings of the 2023 CHI Conference on Human Factors in Computing Systems* (Hamburg, Germany) *(CHI '23)*. Association for Computing Machinery, New York, NY, USA, Article 150, 18 pages. doi:10.1145/3544548.3581422

[58] Anandghan Waghmare, Ishan Chatterjee, Vikram Iyer, and Shwetak Patel. 2024. WatchLink: Enhancing Smartwatches with Sensor Add-Ons via ECG Interface. In *Proceedings of the 37th Annual ACM Symposium on User Interface Software and Technology* (Pittsburgh, PA, USA) *(UIST '24)*. Association for Computing Machinery, New York, NY, USA, Article 14, 13 pages. doi:10.1145/3654777.3676329

[59] Anandghan Waghmare, Ishan Chatterjee, and Shwetak Patel. 2023. Z-Pose: Continuous 3D Hand Pose Tracking Using Single-Point Bio-Impedance Sensing on a Ring. In *Proceedings of the 2nd Workshop on Smart Wearable Systems and Applications* (Madrid, Spain) *(SmartWear '23)*. Association for Computing Machinery, New York, NY, USA, 1–6. doi:10.1145/3615592.3616851

[60] Anandghan Waghmare, Sanjay Varghese, Zhihan Zhang, Ishan Chatterjee, Ritesh Tekriwal, and Shwetak Patel. 2025. Z-Band: On-world Interactions Using Wrist-based Electrical Impedance Sensing. *Proc. ACM Interact. Mob. Wearable Ubiquitous Technol.* 9, 4, Article 216 (Dec. 2025), 45 pages. doi:10.1145/3770637

[61] Saiwen Wang, Jie Song, Jaime Lien, Ivan Poupyrev, and Otmar Hilliges. 2016. Interacting with Soli: Exploring Fine-Grained Dynamic Gesture Recognition in the Radio-Frequency Spectrum. In *Proceedings of the 29th Annual Symposium on User Interface Software and Technology* (Tokyo, Japan) *(UIST '16)*. Association for Computing Machinery, New York, NY, USA, 851–860. doi:10.1145/2984511.2984565

[62] Jason Wiese, T. Scott Saponas, and A.J. Bernheim Brush. 2013. Phoneprioception: enabling mobile phones to infer where they are kept. In *Proceedings of the SIGCHI Conference on Human Factors in Computing Systems* (Paris, France) *(CHI '13)*. Association for Computing Machinery, New York, NY, USA, 2157–2166. doi:10.1145/2470654.2481296

[63] Wikipedia. 2026. 5G NR frequency bands. https://en.wikipedia.org/wiki/5G_NR_frequency_bands Accessed: 2026-03-02.

[64] Wikipedia. 2026. LTE frequency bands. https://en.wikipedia.org/wiki/LTE_frequency_bands Accessed: 2026-03-02.

[65] XDA Developers. 2020. TCL 10 5G gets certified by the FCC with support for mmWave 5G. https://www.xda-developers.com/tcl-10-5g-certified-fcc-support-mmwave-5g-likely-verizon/

[66] Chang Xiao, Karl Bayer, Changxi Zheng, and Shree K. Nayar. 2019. Vidgets: modular mechanical widgets for mobile devices. *ACM Trans. Graph.* 38, 4, Article 100 (July 2019), 12 pages. doi:10.1145/3306346.3322943

[67] Robert Xiao, Scott Hudson, and Chris Harrison. 2016. CapCam: Enabling Rapid, Ad-Hoc, Position-Tracked Interactions Between Devices. In *Proceedings of the 2016 ACM International Conference on Interactive Surfaces and Spaces* (Niagara Falls, Ontario, Canada) *(ISS '16)*. Association for Computing Machinery, New York, NY, USA, 169–178. doi:10.1145/2992154.2992182

[68] Robert Xiao, Greg Lew, James Marsanico, Divya Hariharan, Scott Hudson, and Chris Harrison. 2014. Toffee: enabling ad hoc, around-device interaction with acoustic time-of-arrival correlation. In *Proceedings of the 16th International Conference on Human-Computer Interaction with Mobile Devices & Services* (Toronto, ON, Canada) *(MobileHCI '14)*. Association for Computing Machinery, New York, NY, USA, 67–76. doi:10.1145/2628363.2628383

[69] Robert Xiao, Sven Mayer, and Chris Harrison. 2020. VibroComm: Using Commodity Gyroscopes for Vibroacoustic Data Reception. In *22nd International Conference on Human-Computer Interaction with Mobile Devices and Services* (Oldenburg, Germany) *(MobileHCI '20)*. Association for Computing Machinery, New York, NY, USA, Article 5, 9 pages. doi:10.1145/3379503.3403540

[70] Bin Xu, Yang Li, and Youngwook Kim. 2017. Classification of Finger Movements Based on Reflection Coefficient Variations of a Body-Worn Electrically Small Antenna. *IEEE Antennas and Wireless Propagation Letters* 16 (2017), 1812–1815. doi:10.1109/LAWP.2017.2681099

[71] Jun Yang, Emmanuel Munguia-Tapia, and Simon Gibbs. 2013. Efficient in-pocket detection with mobile phones. In *Proceedings of the 2013 ACM Conference on Pervasive and Ubiquitous Computing Adjunct Publication* (Zurich, Switzerland) *(UbiComp '13 Adjunct)*. Association for Computing Machinery, New York, NY, USA, 31–34. doi:10.1145/2494091.2494099

[72] Hui-Shyong Yeo, Wenxin Feng, and Michael Xuelin Huang. 2020. WATouCH: Enabling Direct Input on Non-touchscreen Using Smartwatch's Photoplethysmogram and IMU Sensor Fusion. In *Proceedings of the 2020 CHI Conference on Human Factors in Computing Systems* (Honolulu, HI, USA) *(CHI '20)*. Association for Computing Machinery, New York, NY, USA, 1–10. doi:10.1145/3313831.3376198

[73] Hui-Shyong Yeo, Gergely Flamich, Patrick Schrempf, David Harris-Birtill, and Aaron Quigley. 2016. RadarCat: Radar Categorization for Input & Interaction. In *Proceedings of the 29th Annual Symposium on User Interface Software and Technology* (Tokyo, Japan) *(UIST '16)*. Association for Computing Machinery, New York, NY, USA, 833–841. doi:10.1145/2984511.2984515

[74] Hui-Shyong Yeo, Erwin Wu, Daehwa Kim, Juyoung Lee, Hyung-il Kim, Seo Young Oh, Luna Takagi, Woontack Woo, Hideki Koike, and Aaron John Quigley. 2023. OmniSense: Exploring Novel Input Sensing and Interaction Techniques on Mobile Device with an Omni-Directional Camera. In *Proceedings of the 2023 CHI Conference on Human Factors in Computing Systems* (Hamburg, Germany) *(CHI '23)*. Association for Computing Machinery, New York, NY, USA, Article 530, 18 pages. doi:10.1145/3544548.3580747

[75] Sang Ho Yoon, Ke Huo, and Karthik Ramani. 2016. TMotion: Embedded 3D Mobile Input using Magnetic Sensing Technique. In *Proceedings of the TEI '16: Tenth International Conference on Tangible, Embedded, and Embodied Interaction* (Eindhoven, Netherlands) *(TEI '16)*. Association for Computing Machinery, New York, NY, USA, 21–29. doi:10.1145/2839462.2839463

[76] Sang Ho Yoon, Yunbo Zhang, Ke Huo, and Karthik Ramani. 2016. TRing: Instant and Customizable Interactions with Objects Using an Embedded Magnet and a Finger-Worn Device. In *Proceedings of the 29th Annual Symposium on User Interface Software and Technology* (Tokyo, Japan) *(UIST '16)*. Association for Computing Machinery, New York, NY, USA, 169–181. doi:10.1145/2984511.2984529

[77] Chun Yu, Xiaoying Wei, Shubh Vachher, Yue Qin, Chen Liang, Yueting Weng, Yizheng Gu, and Yuanchun Shi. 2019. HandSee: Enabling Full Hand Interaction on Smartphone with Front Camera-based Stereo Vision. In *Proceedings of the 2019 CHI Conference on Human Factors in Computing Systems* (Glasgow, Scotland UK) *(CHI '19)*. Association for Computing Machinery, New York, NY, USA, 1–13. doi:10.1145/3290605.3300935

[78] Xiang Zhang, Kaori Ikematsu, Kunihiro Kato, and Yuta Sugiura. 2022. ReflecTouch: Detecting Grasp Posture of Smartphone Using Corneal Reflection Images. In *Proceedings of the 2022 CHI Conference on Human Factors in Computing Systems* (New Orleans, LA, USA) *(CHI '22)*. Association for Computing Machinery, New York, NY, USA, Article 289, 8 pages. doi:10.1145/3491102.3517440

[79] Yang Zhang, Wolf Kienzle, Yanjun Ma, Shiu S. Ng, Hrvoje Benko, and Chris Harrison. 2019. ActiTouch: Robust Touch Detection for On-Skin AR/VR Interfaces. In *Proceedings of the 32nd Annual ACM Symposium on User Interface Software and Technology* (New Orleans, LA, USA) *(UIST '19)*. Association for Computing Machinery, New York, NY, USA, 1151–1159. doi:10.1145/3332165.3347869

[80] Yang Zhang, Gierad Laput, and Chris Harrison. 2017. Electrick: Low-Cost Touch Sensing Using Electric Field Tomography. In *Proceedings of the 2017 CHI Conference on Human Factors in Computing Systems* (Denver, Colorado, USA) *(CHI '17)*. Association for Computing Machinery, New York, NY, USA, 1–14.

doi:10.1145/3025453.3025842

[81] Yang Zhang, Michel Pahud, Christian Holz, Haijun Xia, Gierad Laput, Michael McGuffin, Xiao Tu, Andrew Mittereder, Fei Su, William Buxton, and Ken Hinckley. 2019. Sensing Posture-Aware Pen+Touch Interaction on Tablets. In *Proceedings of the 2019 CHI Conference on Human Factors in Computing Systems* (Glasgow, Scotland UK) *(CHI '19)*. Association for Computing Machinery, New York, NY, USA, 1–14. doi:10.1145/3290605.3300285

[82] Yang Zhang, Junhan Zhou, Gierad Laput, and Chris Harrison. 2016. SkinTrack: Using the Body as an Electrical Waveguide for Continuous Finger Tracking on the Skin. In *Proceedings of the 2016 CHI Conference on Human Factors in Computing Systems* (San Jose, California, USA) *(CHI '16)*. Association for Computing Machinery, New York, NY, USA, 1491–1503. doi:10.1145/2858036.2858082

[83] Junhan Zhou, Yang Zhang, Gierad Laput, and Chris Harrison. 2016. AuraSense: Enabling Expressive Around-Smartwatch Interactions with Electric Field Sensing. In *Proceedings of the 29th Annual Symposium on User Interface Software and Technology* (Tokyo, Japan) *(UIST '16)*. Association for Computing Machinery, New York, NY, USA, 81–86. doi:10.1145/2984511.2984568